Determination of the optical constants of thin films in the visible by static dispersive Fourier transform spectroscopy

A. R. Harvey
Defence Evaluation and Research Agency, St Andrews Road, Malvern, Worcestershire, WR14 3PS, United Kingdom

(Received 19 December 1997; accepted for publication 28 July 1998)

Conventional dispersive Fourier transform spectrometry (DFTS) is a powerful tool for determining optical constants of materials. However, the refined and intrinsically high-cost mechanically scanned interferometers that are necessary are not well suited to use in hostile environments or for time-resolved operation. We describe here a novel approach to DFTS that employs a combination of a Wollaston prism and a linear detector array. It is ideally suited to the precision characterization of thin films with physical thicknesses of up to about 1000 wavelengths or typically about 1 mm. The simplicity and optical efficiency of conventional DFTS are combined with the inherent robustness, superior time resolution, and high repeatability of spatial interferometry. The technique offers an optical throughput that is an order of magnitude higher than spectrophotometry or spectral ellipsometry while accuracies of 1 part in 10^4 and repeatability of 1 part in 10^5 are possible for the measurements of the real part of the refractive index. The imaginary component of the refractive index of thick transparent samples has been measured with an absolute error of less than 2×10^{-4}. The technique may be readily applied from the vacuum ultraviolet to the mid infrared. We present proof-of-principle measurements of optical constants at wave numbers between 9000 and 25 000 cm^{-1} for a self-supporting film of Melinex and for a thin film of ZnSe grown by molecular beam epitaxy onto a glass substrate. © *1998 American Institute of Physics.*
[S0034-6748(98)02210-2]

I. INTRODUCTION

Of the many techniques that may be used to determine the optical constants or optical thicknesses of materials,[1] dispersive Fourier transform spectroscopy (DFTS) offers an alluring array of features.[2–5] Salient advantages include: (1) it is an inherently broadband technique with a very high optical throughput so that the spectral variation of optical constants can be determined more quickly than by competing techniques such as spectrophotometry and spectrometric ellipsometry, (2) the effects of multiple reflections that can be problematic with coherent illumination are easily avoided, (3) the phase and amplitude characteristics imposed on an electromagnetic wave by its interaction with a sample are measured directly and the optical constants are calculated in a simple manner and with lower uncertainties than by other methods. Unfortunately, the Michelson interferometers used for DFTS require considerable refinement and expense and this has tended to restrict its use to the controlled environment of the research laboratory. Furthermore, the temporal resolution of these instruments is limited by the use of mechanically scanned mirrors. The Nyquist criterion requires that the interferogram is sampled for mirror displacements known with a precision of better than one quarter of a wavelength. This becomes increasingly difficult at shorter wavelengths and consequently the DFTS technique has been used mainly in the far infrared where this criterion is more easily met. Where extension of DFTS to visible wavelengths has been reported,[6] a complex laser interferometer and phase-lock-loop system was used to measure the mirror displacements with sufficient accuracy.

We describe here a novel approach to DFTS that yields an inherently robust, and low-cost instrument ideally suited to high-speed and high accuracy measurements of optical constants or optical thickness in hostile environments. It is based upon static Fourier transform spectrometry that exploits the spatial variation in path difference introduced between orthogonally polarized beams propagating through a Wollaston prism.[7–9] The resulting interferograms are formed in parallel, in the spatial domain, enabling single-shot and time-resolved measurements to be made. For general information on spectroscopy using spatial interferometry, see the article by Caulfield.[10] The interferogram spatial wavelengths are of macroscopic dimensions enabling the development of a low-cost Fourier transform spectrometer that can operate at wavelengths as short as the vacuum ultraviolet.[11] The absence of moving parts results in highly repeatable measurements and a very reliable, low-maintenance instrument. We describe the modification of static Fourier transform spectrometry to enable dispersive measurements of the optical constants of thin films. All of the accepted advantages of DFTS over alternative techniques are retained. It is envisaged that the instrument can be usefully employed in hostile environments for the time-resolved measurement of the optical constants or thicknesses of growing thin films or of self-supporting dielectric films. Optical materials and components are available that enable operation for light with wavelengths as short as 120 nm or as long as 7 μm.

 © 1998 American Institute of Physics

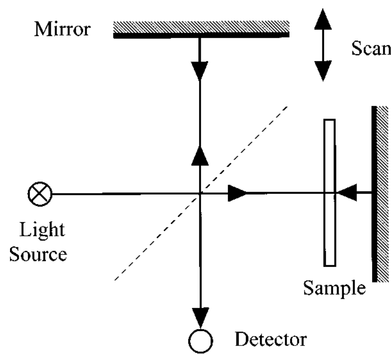

FIG. 1. Conventional DFTS using a mechanically scanned interferometer. The sample is placed in one arm of the interferometer.

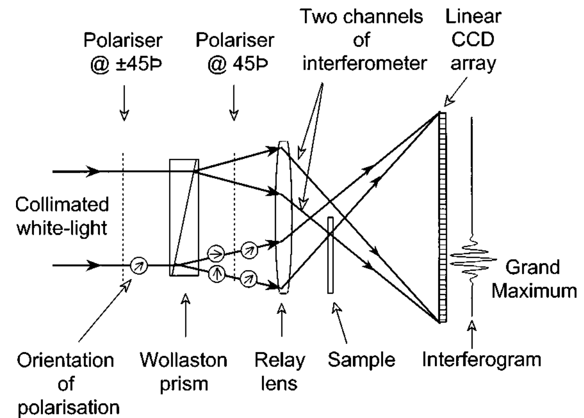

FIG. 2. DFTS using the static Fourier transform spectrometer. The sample is placed at one of the images of the source in the back focal plane of the relay lens.

In Sec. II, the static DFTS technique is described and a simple algorithm for the calculation of the spectral variation of complex refractive index analogous to those used in conventional dispersive Fourier transform spectrometry is presented. This algorithm yields values for the real part of the refractive index with a typical absolute accuracy a few parts in 1000. In Sec. III we discuss the effect and limitations of using an extended white light source with the static DFTS and demonstrate that the optical throughput efficiency of Fourier transform spectroscopy (the so-called Jacquinot advantage), is largely retained. We describe in Sec. IV how systematic errors introduced by imaging aberrations and the geometry of the measurement can be calibrated to reduce uncertainty to less than 0.01%. Instrument calibration is described in Sec. V, random and systematic error budgets are discussed in Sec. VI and in Sec. VII we present proof-of-principle measurements of the optical constants of a thin film of ZnSe grown by molecular beam epitaxy onto a glass substrate and of a free-standing film of Melinex [a poly(tetraphthalate) film similar to Mylar].

II. THEORY

In conventional transmission DFTS, the sample is placed in one arm of a Michelson interferometer as shown in Fig. 1. If the path difference between the arms is scanned with the sample removed, a background white-light interferogram is recorded at the detector that is the Fourier transform of the optical frequency power spectrum of the light source. The interferogram is typified by a grand maximum at the zero path difference (ZPD) position with a modulation that decreases rapidly with increasing path difference. For a DFTS measurement, a sample interferogram is then recorded with the sample located in one arm as shown in Fig. 1. The optical delay introduced by the sample causes the grand maximum of the sample interferogram to be displaced a distance d closer to the beam splitter, where

$$2d=(n-1)t, \tag{1}$$

n is the refractive index of the sample, t is its thickness and it has been tacitly assumed that the sample is nondispersive. For the general case of a dispersive sample, it is convenient to separate the phase differences between the background and sample interferograms into two components: a nondispersive component related by Eq. (1) to the translation of the interferogram and a dispersive component that is determined by the relative phases of each Fourier component of the sample interferogram. Provided that the thickness of the sample is known, the variation of the refractive index with spectral frequency can be calculated from the sum of the dispersive and nondispersive components. In fact, DFTS may be used to calculate the spectral variation of the more general, complex refractive index, $\hat{n}(\sigma)=n(\sigma)+i\kappa(\sigma)$, where $\kappa(\sigma)$ is the extinction coefficient related to the absorption coefficient $\alpha(\sigma)$ by $\kappa(\sigma)=\alpha(\sigma)/4\pi\sigma$ and $\sigma=1/\lambda$ is the wave number of light of wavelength λ. The complex refractive indices and thickness of a planar sample completely determine its complex amplitude transmission and reflection characteristics. For opaque samples, the optical constants can be determined by reflection DFTS in which the sample replaces the fixed mirror.[6]

We will now describe the operation of the static DFTS and how the algorithms employed in conventional DFTS are adapted to enable determination of optical constants. A schematic of the instrument appears in Fig. 2. White light from an extended thermal source such as a tungsten lamp or a discharge lamp is approximately collimated and illuminates the full aperture of the Wollaston prism. This light is polarized by a simple film polarizer oriented at either +45° or −45° to the optic axes of the Wollaston prism. Equal intensities of mutually coherent light are resolved into the ordinary and extraordinary colinearly propagating components within the first wedge of the Wollaston prism. After transmission through the second wedge of the Wollaston prism, there is a path difference[12]

$$\Delta=2b(\sigma)x_W \tan \vartheta \tag{2}$$

between the orthogonally polarized components, where $b(\sigma)=[n_o(\sigma)-n_e(\sigma)]$ is the birefringence of the prism material at wave number σ, $n_o(\sigma)$ and $n_e(\sigma)$ are the ordinary and extraordinary refractive indices of the Wollaston prism material, x_W is the transverse displacement from the center of the Wollaston prism and ϑ is the wedge angle of the Wollaston prism. The spectral variation of birefringence $b(\sigma)$ and of other parameters is indicated here and elsewhere in

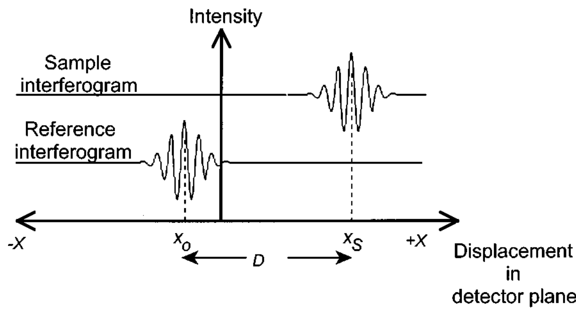

FIG. 3. Schematic sample and reference interferograms.

this article by brackets where it results in a significant change in a calculation. Where it is not significant the brackets are omitted.

The spatial variation in path difference introduced by the Wollaston prism is analogous to the temporal variation introduced by the moving mirrors of a Michelson interferometer and leads to a spatial interferogram localised to a virtual plane within the Wollaston prism. A relay lens forms a real image of the interferogram on a linear detector array and a second polarizer at 45° acts as an analyzer to enable the orthogonally polarized components to interfere. Light of wave number σ forms interference fringes at the detector with spatial frequency[9]

$$v(\sigma)=\frac{2\sigma b(\sigma)\tan\vartheta}{M(\sigma)}, \tag{3}$$

where $M(\sigma)$ is the magnification provided by the relay lens. The discontinuity in refractive index at the wedge interface leads to the mutual divergence of the orthogonally polarized components at an angle[12]

$$\varphi(\sigma)=2b(\sigma)\tan\vartheta, \tag{4}$$

so that each forms a separate image of the source in the back focal plane of the relay lens. The sample to be measured is placed at one of these image points as shown in Fig. 2. Provided that the angular extension of the source is less than φ, there is no overlap of the source images and a sample may be located so as to impart an optical delay to only one ''arm'' of the interferometer. The centers of the two image points are separated by a transverse distance $\varphi(\sigma)f(\sigma)$, where $f(\sigma)$ is the focal length of the relay lens. The instrument is topologically equivalent to a Martin–Puplett interferometer in which the sample is located for single-pass measurement.[13] The standard techniques of DFTS may now be adapted to determine the optical constants or physical thickness of the sample.

Insertion of the sample into one arm of the interferometer increases the optical delay in that arm so that the grand maximum of the interferogram is translated a distance D with respect to the reference interferogram as shown by the schematic interferograms in Fig. 3. The real part of the refractive index may be obtained by inserting Eq. (2) into Eq. (1) to give

$$n(\sigma)=1+\frac{2Db(\sigma)\tan\vartheta}{M(\sigma)t}, \tag{5}$$

If both the sample and the birefringence of the Wollaston prism are nondispersive, then the interferogram is simply translated a distance D without distortion. In reality, the refractive index of the sample and birefringence of the Wollaston prism are both dispersive and the consequent variation of zero path difference position with wave number introduces asymmetry into the sample interferogram and a nonunique definition of D. It is, however, convenient to use a working definition that D is the separation between the grand maxima of the reference and sample interferograms. The spectral variation of the refractive index is calculated from a measurement of the phase shift, $\phi_L(\sigma)$, experienced by each spectral component of light as it propagates sequentially through the Wollaston prism and sample. These phase shifts are identical to the phase shifts of the equivalent spatial frequency components of the spatial interferograms as determined by Eq. (3).

The complex insertion loss $\hat{L}(\sigma)$ of the sample is equal to the ratio

$$\begin{aligned}\hat{L}(\sigma)&=\hat{L}[v(\sigma)]\\&=L[v(\sigma)]\exp\{i\phi_L[v(\sigma)]\}=\frac{\mathrm{FT}^{-1}[I_S(x)]}{\mathrm{FT}^{-1}[I_o(x)]}\end{aligned} \tag{6}$$

of the complex inverse Fourier transforms of the sample and reference interferograms, $I_s(x)$ and $I_o(x)$, where

$$\mathrm{FT}^{-1}[I(x)]=\int_{-X}^{+X} I(x)\exp[-2\pi i v(\sigma)x]dx \tag{7}$$

is the complex inverse Fourier transform of an interferogram and the detector array extends from $-X$ to $+X$.

The phase of $\hat{L}(\sigma)$ is calculated in the usual way from the arctangents of the quotient of the imaginary and real parts of $\phi_L(\sigma)\{=\phi_L[v(\sigma)]\}$. Severe phase branching is avoided by separating $\phi_L(\sigma)$ into a gross shift that can be associated with the relative displacement D of the grand maxima of the two interferograms and a phase $\phi_L'(\sigma)$ associated with the difference between the dispersions of the sample refractive index $n(\sigma)$ and the Wollaston prism birefringence $b(\sigma)$. Rewriting Eq. (5) for this general case, we obtain

$$n(\sigma)=1+\frac{2b(\sigma)\tan\vartheta}{Mt}\left(\frac{\phi_L'(\sigma)}{2\pi v(\sigma)}+D\right). \tag{8}$$

In conventional DFTS, it is usual to record each interferogram symmetrically about the respective grand maxima and take these as the origins for calculation of the Fourier transforms. The analogous step in our instrument would require movement of the detector array and the consequent introduction of a source of error. We have preferred instead to apply the Fourier shift theorem to shift the origins of the inverse Fourier transforms of each interferogram to the positions of their grand maxima.

A highly accurate value for D is not required (it is in any case a weak function of the spectral distribution of the source), since a small error causes a compensatory frequency dependent shift in the phase of $\phi_L'(\sigma)$ so as to produce no net effect in the calculation of $\phi_L(\sigma)^4$. In Eq. (8), $\phi_L'(\sigma)$ is

the principal value of the phase difference between the inverse Fourier transforms of the sample and reference interferograms. If differential dispersion between the sample and the Wollaston prism birefringence is large, it may be necessary to replace $\phi_L'(\sigma)$ by $\phi_L'(\sigma)\pm 2m\pi$, where m is an integer that accounts for phase branching. One may then require *a priori* knowledge of the approximate refractive index of the sample at one part of the spectrum in order to unequivocally obtain values for m. One then assumes a smooth variation in refractive index so that appropriate multiples of 2π may be added or subtracted whenever $\phi_L'(\sigma)$ appears to change discontinuously.

The spectral variation of the extinction coefficient $\kappa(\sigma)$ is obtained by applying Lambert's law and multiplying by a factor that corrects for Fresnel reflections at the two surfaces of the sample:

$$\kappa(\sigma)=\frac{1}{2\pi\sigma t}\ln\left(\frac{4n(\sigma)}{(n(\sigma)+1)^2}\frac{1}{|L(\sigma)|}\right). \tag{9}$$

Measurement of thick samples requires a calibrated compensation plate to be placed in the other arm of the interferometer (that is at the other source image point at the back focal plane of the lens) so that the net path difference remains within the range of the instrument. For example, in the determination of the optical constants of a thin film grown onto a substrate, the sample was positioned so that one of the optical components is transmitted sequentially through the substrate and the thin film and the other is transmitted through the substrate alone. To correct for the Fresnel reflections from the sample in both arms of the interferometer and for attenuation in the substrate, one then uses

$$\kappa(\sigma)=\frac{1}{2\pi\sigma t}\ln\left(\frac{32n_G^2(\sigma)n(\sigma)}{[n_G(\sigma)+1]^3[n_G(\sigma)+n(\sigma)][n(\sigma)+1]}\frac{1}{|L(\sigma)|}\right)-2k_G(\sigma)\frac{t_G}{t}, \tag{10}$$

where $n_G(\sigma)+ik_G(\sigma)$ is the complex refractive index of the substrate and t_G is the substrate thickness. If the substrate is essentially transparent, then the second term in Eq. (10) is equal to zero.

One fundamental difference between conventional DFTS and static DFTS may be noted: in conventional DFTS, the additional optical path length introduced by the sample is compared with a free-space path length, whereas in static DFTS the comparison is with the optical path difference introduced by the birefringence of the Wollaston prism. Dispersion in the birefringence of the Wollaston prism then causes the sample interferogram to be asymmetrical even for a nondispersive sample.

III. OPTICAL THROUGHPUT

The high optical efficiency of Fourier transform spectrometers arises from the so-called Fellget multiplex advantage and the Jacquinot advantage.[3] The first of these refers to the fact that a Fourier transform spectrometer enables all transmitted flux to be detected without the temporal multiplexing that reduces the optical efficiency of a monochromator. Although the static DFTS retains the Fellget advantage, so do modern dispersive spectrometers that also employ detector arrays to simultaneous detect all dispersed flux. However, it should be noted that whereas the instantaneous spectral bandwidth of the static DFTS is limited only by the optical components used and can exceed three octaves, diffractive instruments are limited by higher orders in the diffracted spectrum to unequivocal operation across just one octave. The second advantage, the Jacquinot advantage arises from the large étendue of two-beam interferometers. Typically, a Michelson interferometer will exhibit an étendue 200 times greater than a diffractive instrument of equal resolving power.[3] We will now show that the étendue of a static DFTS, although not as high as for some other two-beam interferometers, is an order of magnitude higher than for a diffractive instrument.

The étendue of an optical system is given by the product of the area of the input aperture and the solid angle field of view Ω. If we consider instruments with input apertures of equal area, the étendue of the conventional and static DFTS instruments can be compared by comparing fields of view. The solid angle field of view of a conventional FTS is $\Omega_M=2\pi/R_M$, where the resolving power $R_M=\sigma\Delta_{\max}$ and $\Delta_{\max}$ is the maximum path difference.[3] The maximum useful angular extension of the light source is that for which the path difference produced by the interferometer for the most oblique rays is a half wavelength different from the path difference for axial rays. As the angular extension of the light source is increased beyond this angle, power is subtracted from the interferogram and there is a consequent reduction in fringe visibility and effective optical throughput. Applying the same criterion to the static DFTS, the maximum field of view subtended by the source at the Wollaston prism should be[12]

$$\Psi_{\text{half wave}}=\sqrt{\frac{n_0^2n_e}{\sigma d(n_e^2-n_0^2)}}, \tag{11}$$

where d is the thickness of the Wollaston prism. Using Eq. (2), the resolving power of the static DFTS can be written as $R_{\text{SDFTS}}=(n_0-n_e)\sigma d$. Combining this with Eq. (11), the solid angle field of view of a static DFTS can then be written as

$$\Omega_{\text{SDFTS}} < \frac{\pi n_0^2 n_e}{R_{\text{SDFTS}}(n_0+n_e)}. \tag{12}$$

For most birefringent materials, this gives a solid angle field of view that is about 65% of that of a Michelson interferometer. This simple analogy is not rigorously valid since the fringes formed by a Michelson interferometer at the detector are circular, whereas, for the static DFTS, the birefringence of the Wollaston prism results in fringes that vary hyperbolically with angle. A more rigorous analysis of this problem yields a value for Ω_{SDFTS} that differs by less than 14% from that obtained using Eq. (12).

For making dispersive measurements, two further factors can limit the field of view: (1) the requirement that the source images in the back focal plane of the relay lens do not overlap and (2) the combined effect of low spatial coherence at the detector with the curvature of the fringe image surface. The first of these effects was mentioned in Sec. II and results in the requirement that the source angular extension Ψ is less than the Wollaston prism splitting angle φ which may be written as

$$\Psi_{\text{splitting}} < \frac{1}{\Delta\sigma X}, \tag{13}$$

where $\Delta\sigma$ is the spectral resolution of the instrument and X is the half width of the Wollaston prism.

The third limitation on field of view arises from the combined effect of the field curvature of the image surface and the partial spatial coherence function of light at the detector array (which is a scaled version of the spatial coherence function at the object plane within the Wollaston prism). Field curvature is a spatially varying longitudinal displacement between the Gaussian image surface and the detector plane. A simple geometrical argument shows that if the two light rays interfering at the detector are traced back toward the source, this longitudinal displacement, Δz, of the image surface from the detector plane is equivalent to a shear

$$\Delta x_W = \frac{2(n_0-n_e)\Delta z \tan\vartheta}{M(M-\Delta z/f)} \approx \frac{2(n_0-n_e)\Delta z \tan\vartheta}{M^2} \tag{14}$$

at the Wollaston prism. Field curvature therefore causes a reduction of fringe visibility for light of partial spatial coherence. From the van Cittert-Zernicke theorem, we can calculate the mutual coherence function and hence the fringe visibility from the source intensity distribution.[14] For a circular, incoherent, and uniform source subtending a half angle Ψ at the Wollaston prism, the fringe visibility for light of wave number σ is

$$V = 2\left|\frac{J_1(2\pi\Psi\sigma\Delta x_W)}{2\pi\Psi\sigma\Delta x_W}\right|, \tag{15}$$

where J_1 is a first-order Bessel function. The visibility of the fringe envelope therefore has its first zero when the interfering components are sheered by a transverse distance $\Delta x_\gamma = 1.22/2\sigma\Psi$. For a simple lens, the longitudinal displacement of the curved image surface from the Gaussian image plane at transverse displacement x_I in the image plane is $\Delta z = x_I^2/2n_L f$, where n_L is the refractive index of the lens material.[15] Combining this with Eqs. (14) and (15) and requiring that for temporally coherent illumination, the visibility at the edge of the detector is greater than 0.5 yields the condition

$$\Psi_{\text{coherence}} < \frac{2.215 n_L f M^2}{\pi X R}. \tag{16}$$

We now consider the relative severity of the limiting fields of view $\Psi_{\text{half wave}}$, $\Psi_{\text{splitting}}$, and $\Psi_{\text{coherence}}$ based upon typical system parameters. For a detector array with N pixels, the maximum resolving power for Nyquist sampling of the interferogram is $N/4$ so that for a 4096 element silicon detector with useable sensitivity between 10 000 and 25 000 cm^{-1}, we obtain a maximum resolving power R_{SDFTS} of approximately 1000 at high wave numbers and 400 at low wave numbers. The resolution will be approximately 25 cm^{-1} at all wave numbers. The maximum field of view of the Wollaston prism is the high wave number value of $\Psi_{\text{half wave}}$ which is 65 mrad. This is the limiting half-angle source extension for nondispersive static Fourier transform spectroscopy.

We next consider the two additional limitations on source extension particular to the application of static Fourier transform spectroscopy in its dispersive mode. Assuming that the Wollaston prism will have lateral dimensions similar to that of the detector array, we can insert a typical value of 14 mm for X into Eq. (13) to give $\Psi_{\text{splitting}} \approx 28$ mrad.

To calculate $\Psi_{\text{coherence}}$, we can assume $M \approx 1$ and $n_L \approx 1.5$ to give $\Psi_{\text{coherence}} \approx 0.076 f$ mrad. Thus provided the focal length of the lens is greater than 371 mm, $\Psi_{\text{coherence}}$ will be greater than $\Psi_{\text{splitting}}$. In conclusion, $\Psi_{\text{coherence}}$ and $\Psi_{\text{splitting}}$ are typically smaller than $\Psi_{\text{half wave}}$ which limits the solid-angle field of view to typically 12% of the field of view of a DFTS based on a Michelson interferometer. For a Michelson interferometer, 50% of the flux is transmitted to the detectors on average and for the static interferometer described here, the use of polarizers limits the transmitted flux to 25%. In principle, reflective polarizers could replace thin film polarizers and the reflected light could be used so as to give 100% optical efficiency for the static DFTS, but this would incur considerable added (probably unjustifiable) complexity. The overall optical throughput of the static DFTS is thus about 6% of that of a Michelson-based DFTS. Conventional Fourier transform spectroscopy offers an étendue 200 times greater than a dispersive instrument[3] so static DFTS can be seen to offer an étendue this is at least an order of magnitude higher than a dispersive device as used by competing methods such as spectrophotometry or spectroscopic ellipsometry. Furthermore, because DFTS directly measures the field transmitted through the sample rather than the optical intensity (that is, it is a homodyning rather than total-power technique), a greater dynamic range is obtained from the detector.

IV. CALIBRATION OF ABERRATIONS

The algorithms described in Sec. II can be used to measure optical delay with an absolute accuracy of a few parts in 1000. Several systematic errors of about this relative magni-

tude are introduced by imaging aberrations and the non-normal incidence of the light transmitted through the sample. In this section we describe how systematic errors can be calibrated to give very significant reductions in the measured uncertainty in optical delay.

A. Non-normal transmission through sample

It is apparent from Fig. 2 that light rays at some calibration wave number $\sigma_{\rm cal}$ arriving at the detector array at displacement x have a slope of $\tan^{-1}[x/M(\sigma_{\rm cal})f(\sigma_{\rm cal})]$ with respect to the optical axis. This increases the effective thickness of the sample. At a different wave number σ, chromatic aberration will introduce a small change in this angle to $\tan^{-1}\{x/[M(\sigma_{\rm cal})f(\sigma_{\rm cal})+f(\sigma_{\rm cal})-f(\sigma)]\}$. Snell's law refraction within the sample means that for a sample of thickness t, oblique rays traverse a physical thickness in the sample equal to

$$t\left[1+\left(\frac{x}{n(\sigma)f(\sigma_{\rm cal})M(\sigma_{\rm cal})+f(\sigma_{\rm cal})-f(\sigma)}\right)^2\right]^{1/2}. \quad (17)$$

B. Imaging aberrations

The relay lens introduces a magnification that varies parabolically with both wave number σ and transverse displacement x. To a first order, this variation may be accurately described by

$$M(x,\sigma)\cong M(0,\sigma_{\rm peak})[1-\chi(\sigma-\sigma_{\rm peak})^2](1+\xi x^2), \quad (18)$$

where χ and ξ describe the degree of chromatic and geometrical distortion, respectively, and may be determined empirically. The value $M(0,\sigma_{\rm peak})$ is the peak in the spectral variation of magnification (at $x=0$) that occurs at $\sigma=\sigma_{\rm peak}$. The dominant effect of this distortion is the translation of the grand maxima of the reference and sample interferograms.

C. Calibrated determination of optical constants

A more accurate calculation of refractive index may now be obtained by substituting Eqs. (17) and (18) into Eq. (8). For accurate determination of $n(\sigma)$, one must also include the fact that the refractive index of air, $n_{\rm air}(\sigma)$, is slightly greater than unity (about 1.0003 for green light). Thus we obtain

$$n(\sigma)\approx n_{\rm air}(\sigma)+\frac{2b(\sigma)\tan\vartheta}{t\left[1+\left(\frac{x_S}{n(\sigma)f(\sigma_{\rm cal})M(\sigma_{\rm can})+f(\sigma_{\rm cal})-f(\sigma)}\right)^2\right]^{1/2}M(0,\sigma_{\rm peak})[1-\chi(\sigma-\sigma'_{\rm peak})^2]}$$
$$\times\left\{\frac{1}{2\pi\nu}(\phi_S-\phi_O)+x_S-x_O+\xi\left[\frac{1}{2\pi\nu}(\phi_S x_S^2-\phi_O x_O^2)+x_S^3-x_O^3\right]\right\}, \quad (19)$$

where x_S and x_O denote the x coordinates of the grand maxima of the sample and background interferograms, respectively.

The refractive indices are calculated at a set of discrete wave numbers σ_p that correspond to the spatial frequencies v_p obtained from the discrete Fourier transforms of the sample and reference interferograms, where p is an index running from zero to $N/2$ and N is the number of pixels used to sample the interferograms. It will be noticed that in Eq. (19) the refractive index also appears on the right-hand side, but since the refractive index will generally be smoothly varying, it is possible when calculating $n(\sigma_p)$, to substitute one of the neighboring values $n(\sigma_{p\pm1})$ into the right-hand side without significant loss of accuracy.

The above corrections for the imaging distortion and the non-normal incidence are multiplicative and are at the level of a few parts in one thousand for our demonstration system. The magnitudes of both corrections are reduced by using a longer focal length relay lens. The values of χ and ξ may also be minimized by using imaging configurations in which image and object halves of the imaging system are similar. An example is the use of an achromatic triplet optimized for and used in a 1:1 imaging conjugation. In principle, distortion and the chromatic variations of distortion are then reduced to zero.

V. CALIBRATION

Calculation of the optical constants using Eqs. (8)–(10) requires the calibration of the birefringence $b(\sigma)$, the wedge angle ϑ of the Wollaston prism, and a measurement of the nominal magnification $M(0,\sigma)$. More accurate calculation using Eq. (19) requires the additional calculation of the constants χ, ξ, and $\sigma_{\rm peak}$. For a broadband source, we are faced with the recursive problem that the mapping of interferogram spatial frequency to wave number can only be calculated if $b(\sigma)$ and $M(0,\sigma)$ are known, but these parameters are themselves dependent on wave number. This problem has been tackled by building an interpolated look-up table between spatial frequency and equivalent wave number as follows:

(i) Tabulated values of birefringence obtained from the literature are used to derive an interpolating function that enables the calculation of birefringence at arbitrary wave numbers.

(ii) The Wollaston prism is replaced by a Ronchi grating enabling $M(0,\sigma)$ to be measured at discrete wave numbers defined by interference filters. A least-squares quadratic fit to this data enables χ, σ_{peak}, and $M(0,\sigma_{\mathrm{peak}})$ to be calculated.

(iii) The spectrometer is illuminated by light from a coherent reference source such as a helium neon laser. A least-squares fit to the spatial frequency chirp of the interferogram enables the calculation of the distortion parameter ξ.

(iv) The spatial frequency of fringes v_{cal} is measured for the reference source of wave number σ_{cal}.

We are now able to evaluate a calibration constant

$$\beta=\frac{1-\chi(\sigma_{\mathrm{peak}}-\sigma_{\mathrm{cal}})^2}{b(\sigma_{\mathrm{cal}})}\frac{\nu_{\mathrm{cal}}}{\sigma_{\mathrm{cal}}}, \tag{20}$$

which from inspection of Eqs. (3) and (12) may also be written as

$$\beta=\frac{2\tan\vartheta}{M(0,\sigma_{\mathrm{peak}})(1+\xi^2x)}. \tag{21}$$

Combining Eqs. (3), (20), and (21) yields the expression

$$\nu(\sigma)=\frac{b(\sigma)}{1-\chi(\sigma-\sigma_{\mathrm{peak}})^2}\beta\sigma \tag{22}$$

for the spatial frequency of fringes formed by light of wave number σ. The need for accurate determination of the absolute value of $M(0,\sigma_{\mathrm{peak}})$ and ϑ is thus obviated.

A look-up table of values σ_p is calculated by interpolation of Eq. (22) for all discrete values of $\nu_p=p/N\delta$, where δ is the pitch of the detector array, N is the number of pixels in the array, and p runs from zero to $N/2$. We can now write

$$\sigma_p=\mathscr{Y}(p), \tag{23}$$

where $\mathscr{Y}$ represents the look-up function. Periodic calibration of the instrument consists simply of the recalculation of β from the measurement in step (iv) above to allow for thermal drift of the spectrometer. For uniform illumination of the Wollaston prism, the transverse variation in magnification has no effect on the value of β.

VI. ERRORS

Systematic errors in the determination of σ and $n(\sigma)$ are dominated by the following uncertainties:

(i) Tabulated values of birefringence $b(\sigma)$ for the common birefringent materials can be found in the literature with typical uncertainties of the order of 1 part in 10^3. The absolute value of birefringence at any one wave number is not important since it is absorbed into the calibration constant β. Of greater importance is the relative spectral variation of birefringence with respect to a reference value at wave number σ_{cal} and this may be calibrated with an accuracy of about 1 part in 10^5.

(ii) For most materials, birefringence changes by about 1 part in 10^4 per °C of temperature drift.

(iii) If the determination of the thickness of a sample can be made with an accuracy of about 1 nm, this will introduce an error of 1 part in 10^5 for a 100 μm thick sample and 1 part in 10^3 for a 1 μm thick sample.

(iv) The calibration factors χ and ξ can be measured with a repeatability of about 1 part in 10^2. This corresponds to a worst case maximum error of less than 1 part in 10^5 in the calculation of refractive index.

(iv) The calibration factor β can be measured with a repeatability of approximately 1 part in 10^5.

For thin (1 μm) samples, the absolute uncertainty in $n(\sigma)$ is clearly dominated by the uncertainty in sample thickness. For thick (100 μm) samples, the uncertainty in the spectral variation of the birefringence dominates. Calibration of this latter effect by accurate measurement of the spectral variation of $\nu(\sigma)$ enables the determination of $n(\sigma)$ to be made with an absolute uncertainty of about 1 part in 10^5 for thick samples and 1 part in 10^3 for thin samples. Drift in temperature of about 0.1 °C between calibration and measurement will introduce additional errors of about 1 part in 10^5.

For some applications, it is the repeatability of a measurement that is of greatest importance. The dominant limitations on repeatability arise from two main effects; temperature drift of the Wollaston prism as described above and electrical noise on the detector output. Simultaneous calibration using a spectral reference such as a laser can reduce the error due to temperature drift to below the fundamental limit determined by noise on the detector output. This limit is considered next.

Fourier transformation of the measured interferogram signal gives a frequency spectrum accompanied by broadband noise that arises from fixed pattern noise in the optics and random detector noise. Each spectral component in the spectrum of the detected interferogram can be considered as a sum of three electrical phasors; a pure stationary carrier signal representing the noise-free interferogram, a fixed pattern noise phasor and a noise phasor with random phase distributed uniformly in the interval $-\pi$ to $+\pi$, and an amplitude with a stochastic variation determined by the noise character. The resultant phasor suffers both amplitude and phase modulation by the random noise. For large signal-to-noise ratios, the resultant uncertainty $\Delta\phi$ in the phase is given by[16]

$$\overline{\Delta\phi^2}=\frac{N_0}{2S}, \tag{24}$$

where N_0/S is the ratio of the electrical noise power to the electrical signal power in one resolution bandwidth. The factor of two arises because on average, only half of the noise power contributes to phase modulation of the signal (the other half contributes to amplitude modulation). Transmission of light of wave number σ through a sample of thickness t changes its phase with respect to vacuum propagation by an amount $\phi=2\pi\sigma(n-1)t$. Differentiating ϕ with respect to n and combining this with Eq. (24) gives the predicted uncertainty in the determination of refractive index due to random additive noise to be

$$\Delta n(\sigma)=\frac{1}{2\pi\sigma t}\sqrt{\frac{N_0[\nu(\sigma)]}{S[\nu(\sigma)]}}. \tag{25}$$

For a typical electrical signal-to-noise ratio of 40 dB and a broadband optical spectrum, Eq. (25) gives a typical uncertainty of 10^{-4} for thin samples and 10^{-6} for the thickest samples that can be measured simply by the DFTS described here. In terms of the determination of optical thickness, this suggests a noise equivalent error of the order of a nanometer in each spectral resolution bandwidth which is comparable to the assumed absolute accuracy with which the sample could be measured. If the complete spectrum is used to calculate sample thickness, then this figure would be further reduced by the weighted square root of the effective number of measurements which provides the potential to measure displacement with a repeatability measured in picometers. It may not always be necessary to independently measure sample thickness, since, as is mentioned in the next section, it is possible to simultaneously determine refractive index and thickness using DFTS.

Uncertainties in the absolute measurement of $\kappa(\sigma)$ arise when the differences between sample and reference interferograms are not due solely to Fresnel reflections at the sample surfaces and absorption within the sample. Several systematic factors are common to recording both the sample and reference interferograms and so cancel when the ratio $\hat{L}(\sigma)$ in Eq. (6) is calculated. These include fixed pattern noise in the optics and at the detector, the detector MTF, the spectral transmission of the optical components, and the spectral responsivity of the detector. Factors that can introduce uncertainty in $\kappa(\sigma)$ are those that are not common to both interferograms and include the optical quality and cleanliness of the sample, stability of the source intensity, spectral stability of the optical transmission path, and stability of detector responsivity. These sources of error do not lead to a simple and general theoretical analysis and are not considered here in detail.

However, for a transparent sample $\kappa(\sigma)$ is equal to zero and this is the value that should be measured after correction of the Fresnel losses calculated from the measured variation of refractive index. Thus an indication of the accuracy of the measured value of $\kappa(\sigma)$ can be estimated by the closeness to zero of the measured value for an ostensibly transparent sample. As shown in the next section, the static DFTS yielded values for $\kappa(\sigma)$ in the transparent regime that, for a thick sample, were typically less than 10^{-4} with random variations from the mean less than 10^{-5}.

VII. EXPERIMENTS

Two proof-of-principle measurements of complex refractive indices that demonstrate the application of static DFTS are presented in this section. The first is for a thin film of ZnSe grown onto a glass substrate by molecular beam epitaxy and the second is for a free-standing Melinex film. The experimental details are described below.

The Wollaston prism is fabricated from calcite and has a wedge angle of $\vartheta = 2.5°$ and a width of 20 mm. Ideally, the relay lens, which is a 125 mm focal length, achromatic triplet optimized for finite conjugate imaging, would be used at unity magnification since this configuration yields zero distortion. However, we chose a magnification of approximately 1.5 to match the 28.672 mm wide detector array to the image of the Wollaston prism and this introduced a small amount of pincushion distortion. The spectral and transverse variations in the imaging magnifications were calibrated using the methods described in Sec. V. A least-squares fit to the spectral variation of magnification gave a value of $\chi = 1.3 \times 10^{-10}$ cm^2 resulting in a maximum variation of less than 0.5% across the spectral range. A value of $\xi = 1.2 \times 10^{-5}$ mm^{-2} was measured for the distortion parameter which translates to a maximum distortion of 0.24% in displacement and 0.74% in spatial frequency at the edge of the detector.

The Wollaston prism used introduces a maximum path difference of ± 150 μm yielding a full width half maximum resolution of 60 cm^{-1}. The resulting Nyquist sampling criterion requires the high wave number cutoff to be less than 67 000 cm^{-1} and this is ensured by the 25 000 cm^{-1} high wave number cutoff of the silicon CCD detector array. The low wave number cutoff of 9000 cm^{-1} is also determined by the spectral responsivity of the detector. The linear detector array was a 2048-element CCD array that is interfaced via a 13-bit analog-to-digital converter to a personal computer. The temporal resolution was limited to a maximum frame rate of 30 Hz by the 100 kHz maximum sample rate of the analog-to-digital converter. At these frame rates real-time calculation of optical constants is possible using a modest computer.

Calculating the maximum half-angle fields of view given by Eqs. (12), (13), and (16), the maximum angular source extensions at $\sigma = 25\,000$ cm^{-1} are $\Psi_{\text{half wave}} = 57$ mrad, $\Psi_{\text{splitting}} = 12$ mrad, and $\Psi_{\text{coherence}} = 34$ mrad. That is to say that for this proof-of-principle system, the source extension is limited to 12 mrad by the necessity to separate the images of the source at the sample location. The optical source was an optically attenuated 50 W quartz halogen lamp stopped down to give source half-angle extensions of typically 0.4 mrad. We estimate that for an optimized instrument, similar measurements could be made with less than 10% of this optical power.

The fringe visibility for these measurements was calculated to be reduced by no more than 1% at the extremes of the linear detector array and for the actual locations of the sample and reference interferograms, was less than 0.2%. Although it is possible in principle to calibrate the effects of reduced fringe visibility to give more accurate determination of sample absorption, the exact calibration is complicated by the dependence of the visibility function on the detailed source intensity distribution. The fringe visibilities for this demonstration measurement are so close to unity that calibration does not significantly improve accuracy.

Two interferograms are recorded for each sample and reference interferogram: $I^+(x)$ with the input polarizer oriented at $+45°$ and $I^-(x)$ with the input polarizer oriented at $-45°$. Calculation of the normalized interferogram, $I(x) = [(I^-(x) - I^+(x)]/[(I^-(x) + I^+(x)]$, results in the subtraction of the interferogram bias, attenuation of fixed pattern noise (by 26 dB in the electrical domain for this experiment) and reduced sensitivity to nonuniform illumination of the Wollaston prism 8. If unnormalized interferograms are used

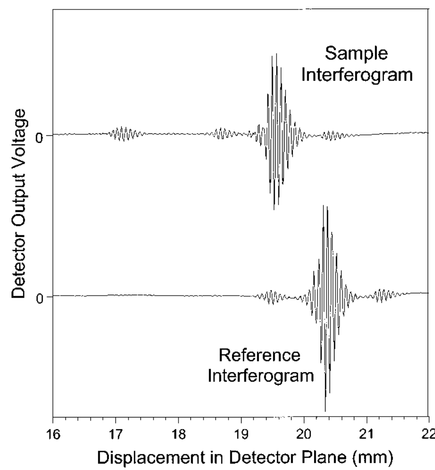

FIG. 4. Sections of the reference and sample interferograms for the measurement of a 4.88 μm thick thin film of ZnSe. Interference effects due to second-order reflection within the ZnSe film are evident on the sample interferogram at 17 mm.

and there is a change in source intensity between recording sample and reference interferograms then the value of $|L(\sigma)|$ used in Eqs. (9) and (10) would be scaled by the intensity change leading to a systematic error in $\kappa(\sigma)$. Use of normalized interferograms reduces this sensitivity, although the magnitude of this improvement is dependent upon the relative time scales of lamp intensity variations and the intervals between recording the four interferograms.

The thin film sample measured was a 4.88 μm thick layer of ZnSe grown by molecular beam epitaxy onto a 1 mm thick glass substrate. The thin film was surrounded by a border on which no thin film was grown. The sample was positioned in the back focal plane of the relay lens so that the reference light channel passed through the border (and thus through the glass substrate only) and the sample channel passed through the glass substrate and the ZnSe thin film in sequence. On the assumption that the glass substrate was uniformly flat, the glass border in the reference channel compensated for the glass in the sample channel. Normalized sample and reference interferograms were recorded with the sample in place and with it absent and these are shown in Fig. 4.

Second-order interference caused by double reflection within the ZnSe film is apparent in the sample interferogram at a displacement of 2.5 mm to the left of the grand maximum. Although these second-order interference effects enable the sample thickness to be calculated,[17] this was not done here and the second-order interferogram was removed by manual editing prior to Fourier transformation.

The real and imaginary refractive indices $n(\sigma)$ and $\kappa(\sigma)$ calculated from the data of Fig. 4 are shown in Fig. 5. The optical constants of ZnSe have been measured previously by spectroscopic ellipsometry of single crystals[18] and of thin films grown by MBE.[19] Measurements of $n(\sigma)$ taken from Fig. 5 of Ref. 18 are superimposed in Fig. 5 and show excellent agreement (within the accuracy of the transcription of the data from the graph).

The imaginary part of the refractive index, $\kappa(\sigma)$, is shown to be ostensibly zero between the low wave number

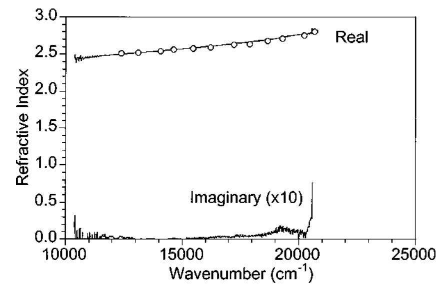

FIG. 5. Real and imaginary components of ZnSe refractive indices as measured by static DFTS. The open circles show the measurements transcribed from Fig. 5 of Ref. 18.

limit of the measurement at 10 400 and 20 500 cm^{-1} apart from a small monotonic increase with wave number which which is probably due to scattering from surface defects and contamination. A slight peak of 0.003 in $\kappa(\sigma)$ is apparent at 19 300 cm^{-1} and coincides with an increase of 0.003 above the general trend of $n(\sigma)$ at the same wave number. This may be due to a weak resonance in this sample of ZnSe. This feature is not apparent in a previous report on the optical constants of ZnSe[18] since it falls between the much more widely spaced data points in that article. Above 20 500 cm^{-1}, $\kappa(\sigma)$ rises rapidly to about 0.03 at 20 800 cm^{-1} corresponding to 2% transmission by the sample which is equal to the system dynamic range at this wave number. The system dynamic range drops off sharply with increasing wave number due to the diminishing output of the quartz-halogen lamp and the falling sensitivity of the silicon detector so that optical transmission by the thin film beyond 20 800 cm^{-1} is below the noise floor. This absorption feature is due to a transition in the energy band structure of ZnSe at 2.69 eV that results in a peak value in $\kappa(\sigma)$ of approximately 0.37 at 21 700 wave numbers.[18] For optically thick and opaque regions of the spectrum such as this, reflection DFTS is more appropriate.[4]

Measurements have also been made on a free-standing film of Melinex [the ICI brand name for poly(tetraphthalate)]. DuPont manufacture a similar, though not identical poly(tetraphthalate) film under the brand name of Mylar. The Melinex film was measured mechanically to have a thickness of 105.7$\pm$0.5 μm. The measurement of a free-standing film such as this is more straight forward than for a supported film since no allowance need be made for the effects of a substrate.

The calculated optical constants of the Melinex film are shown in Fig. 6. The magnitudes of these results are quite

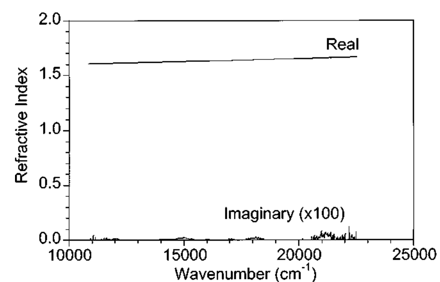

FIG. 6. Measured refractive indices of a free-standing film of Melinex.

dissimilar from results published for Mylar.[20] This is not unexpected since Mylar and Melinex are not identical (for example, Mylar is birefringent whereas Melinex is not) and there can in any case be significant sample-to-sample variability of the optical constants of nominally identical polymers.[21]

The low wave number limit of the Melinex measurement is similar to that obtained for the ZnSe sample, but due to the greater high wave number transparency of Melinex, the high wave number measurement limit is extended to the system cutoff at 23 400 cm^{-1}.

In all of the optical intensity spectra recorded with the static DFTS, a channeled-spectrum modulation was apparent on the continuum. This is believed to be due to etalon effects within either the detector or film polarisers. In these experiments, thermal drift of the channeled-spectrum between recording interferograms has resulted in channeled-spectrum artifacts on the $\kappa(\sigma)$ curves shown in Figs. 5 and 6. The amplitude of these artefacts is about 10^{-3} for the ZnSe measurement and 10^{-4} for the Melinex measurement. In principle, these systematic errors can be avoided by thermal stabilization. There is no significant related effect on the curves for $n(\sigma)$. Random noise on the traces of $\kappa(\sigma)$ are approximately 2×10^{-4} for the measurement of ZnSe and 10^{-5} for the measurement of Melinex.

Random noise on the $n(\sigma)$ curves is due to random noise on the detector output and its magnitude, as predicted by Eq. (25), increases toward the spectral extremes where the signal-to-noise ratio is poorer. The signal-to-noise ratio for the sample spectra reaches a maximum of 40 dB (electrical domain) close to 13 000 cm^{-1} and the random variation in $n(\sigma)$ at this point is 2.4×10^{-4} for ZnSe and 1.5×10^{-5} for Melinex. This corresponds to 1 part in 10^4 and 1 part in 10^5, respectively, and is in agreement with the expected random errors predicted by Eq. (25).

VIII. DISCUSSION

The static DFTS as described offers several advantages over conventional approaches to static DFTS and has been patented[22] with the intention of developing a commercial, general purpose instrument. The instrument is made possible by the availability of high quality linear detector arrays, but the specifications of the available arrays is a limiting factor. In particular, the maximum thickness of sample that can be measured is limited to the displacement of the interferogram that can be measured and this is determined by the number of pixels available. For a 2048-element array, the maximum thickness of a sample with that can be measured is 1 mm when the refractive index is 2 and the wavelength is 1 μm. Several methods can be conceived for increasing the thickness range, such as using calibrated compensation plates, contiguous linear arrays, or two-dimensional arrays with custom designed birefringent prisms.

Additional limitations due to detector arrays are the maximum pixel rate (which typically limits the temporal resolution to about 100 μs) and high cost for operation outside of the sensitivity range of silicon. For some applications, such as process control and thickness monitoring that do not require a general purpose instrument, it may be attractive to employ optical masks and integrating detection not unlike the Van der Lugt correlators used in Fourier optics.[22] This offers scope for cost reductions, improvements in temporal resolution, and improved sensitivity, but with the loss of the flexibility provided by electronic processing.

ACKNOWLEDGMENTS

The author is grateful to M. J. Padgett of the University of St. Andrews, U.K. for useful discussions. This research was supported by the U.K. Ministry of Defence.

[1] See, for example, E. D. Palik, *Handbook of Optical Constants of Solids* (Academic, London, UK, 1985).
[2] J. Chamberlain, J. E. Gibbs, and H. A. Gebbie, Infrared Phys. **9**, 185 (1969).
[3] R. J. Bell, *Introductory Fourier Transform Spectroscopy* (Academic, New York, 1972), Chap. 8.
[4] J. R. Birch and T. J. Parker, in *Infrared and Millimetre Waves*, edited by K. J. Button (Academic, New York, 1979), Vol. 2, Chap. 3.
[5] T. J. Parker, Contemp. Phys. **31**, 335 (1990).
[6] N. J. Burton and T. J. Parker, J. Mod. Opt. **36**, 1103 (1989).
[7] M. J. Padgett, A. R. Harvey, A. J. Duncan, and W. Sibbett, Appl. Opt. **33**, 6035 (1994).
[8] A. R. Harvey, M. Begbie, and M. J. Padgett, Am. J. Phys. **62**, 1033 (1994).
[9] M. J. Padgett and A. R. Harvey, Rev. Sci. Instrum. **66**, 2807 (1995).
[10] H. J. Caulfield, in *Advances in Holography*, edited by N. S. Farhat (Marcel Decker, New York, 1976), Vol. 2, pp. 141–184.
[11] J. Courtial, B. A. Patterson, W. Hirst, A. R. Harvey, A. J. Duncan, W. Sibbett, and M. J. Padgett, Appl. Opt. **36**, 1901 (1997).
[12] M. Françon and S. Mallick, *Polarization Interferometers* (Wiley, London, 1972).
[13] D. H. Martin, in *Infrared and Millimetre Waves*, edited by K. J. Button (Academic, New York, 1982), Vol. 6, Chap. 2.
[14] M. Born and E. Wolf, *Principles of Optics*, 6th ed. (Pergamon, Oxford, England, 1987).
[15] L. Levi, *Applied Optics* (Wiley, New York, 1968), Vol. 1.
[16] W. P. Robins, *Phase Noise in Signal Sources* (Peter Peregrinus, London, UK, 1984).
[17] J. R. Birch, *Mikrochim Acta*, Vol. III (Springer, Wien, 1987), pp. 105–122.
[18] S. Adachi and T. Taguchi, Phys. Rev. **43**, 9569 (1990).
[19] R. Dahmani, L. Salamanca-Riba, N. V. Nguyen, D. Chandler, B. Horowitz, and T. Jonker, J. Appl. Phys. **76**, 514 (1994).
[20] Z. Seres, A. Galonsky, K. Leki, J. J. Kruse, and P. D. Zecher, Opt. Eng. **33**, 3031 (1994).
[21] J. R. Birch, J. D. Dromney, and J. Lesurf, National Physical Laboratory Report DES 69, 1981.
[22] M. J. Padgett, A. J. Duncan, W. Sibbett, and A. R. Harvey, U.K. Patent GB 2294778B, 22/10/97.